Geophys. J. Int. (1999) **139,** 645–656

Ice flow physical processes derived from the ERS-1 high-resolution map of the Antarctica and Greenland ice sheets

Frédérique Rémy,[1] Philippe Shaeffer[2] and Benoît Legrésy[1]

[1] *Legos (CNES-CNRS-UPS),* 18 *avenue E. Belin,* 31401 *Toulouse Cedex* 4, *France. E-mail: Frederique.Remy@cnes.fr*
[2] *CLS/CNES,* 8–10 *rue Hermes, Parc Technologique du canal,* 31526 *Ramonville St Agne, France*

Accepted 1999 July 7. Received 1999 June 7; in original form 1998 June 24

SUMMARY

The ERS-1 satellite, launched in 1991, has provided altimetric observations of the Greenland Ice Sheet and 80 per cent of the Antarctica Ice Sheet north of 82°S. It was placed in a geodetic (168-day repeat) orbit between April 1994 and March 1995, yielding a 1.5 km across-track spacing at latitude 70° with a higher along-track sampling of 350 m. We have analysed the waveform altimetric data from this period to compute maps with a 1/30° grid size. Data processing consists of correcting for environmental factors and editing and retracking the waveforms. A further step consists of reducing the radial orbit error through crossover analysis and correcting the slope error to second order. The high-resolution topography of both ice sheets reveals numerous details. A kilometre-scale surface roughness running at 45° from the flow direction is the dominant topographic characteristic of both continents. Antarctica also exhibits many scars due to local flow anomalies. Several physical processes can be identified: abrupt transitions from deformation to sliding and vice versa, and impressive strike-slip phenomena, inducing *en echelon* folds.

Key words: rheology, satellite geodesy, topography.

1 INTRODUCTION

Ice sheet surface topography plays an important role in ice sheet dynamics, flow and balance studies. This is due to the result of a balance between snow accumulation and ablation and ice flow above bedrock. Therefore, surface topography contains a signature of the main physical processes (climatic and dynamic) that act on an ice sheet. As the viscosity and thermal inertia are large, the current topography results from the climatic and dynamic history over the last few tens of thousands of years. It is also an initial condition for the future evolution. The large-scale topography controls flow direction and its mapping allows the derivation of the balance velocity. Moreover, the deformation and sliding velocities depend on the basal shear stress and thus on surface slopes. Accurate information about the topography is thus crucial in the prediction of the future evolution and in furthering our knowledge of ice dynamics, either by providing an empirical parametrization of the flow law or by pointing out unknown physical processes. From the small scale to the large scale, topography contains important information on local anomalies or on general trend behaviour, which can be inverted from precise topography (Rémy *et al.* 1996).

From the first *in situ* observations, two main topographic characteristics were observed: the large-scale parabolic shape of ice sheets, predicted by Orovan (1949), and medium-scale surface undulations. The parabolic shape was theoretically explained by Glen (1955), whilst the surface undulations were related to bedrock topography perturbations, reduced by a damping factor that depends on ice thickness, velocity, viscosity and undulation wavelengths (Budd 1970). The first regional topography maps were derived from aircraft surveys for Terre Adelie land (in 1974) or from balloons (in 1982) prior to the first satellite radar altimetry map (Brooks & Norcross 1982). Owing to the size and climatological conditions of an ice sheet, satellite altimetry provides a powerful tool for surface observations. The first studies made with the Seasat altimeter (Zwally *et al.* 1983; Cudlip & McIntyre 1986; Rémy *et al.* 1989) were able to distinguish characteristic surface features linked to the flow: flat surface areas related to subglacial lakes or 20-km-scale undulations related to bedrock. These observations were available only over southern Greenland and over a small region of Antarctica to the north of 72°S.

The ERS-1 satellite was launched in 1991 by the European Space Agency to study the Earth's environment. Its spatial coverage between 82°N and 82°S provides for the first time altimetric observations of the whole Greenland Ice Sheet and 80 per cent of the Antarctic Ice Sheet. It was initially placed in 3- and 35-day repeat orbits, up to April 1994. The launch of ERS-1 allowed a much greater area to be viewed than was

previously possible and, for instance, the discovery of the large areal extent of Vostok Lake (Ridley *et al.* 1993; Kapitsa *et al.* 1996), the mapping of the characteristic kilometre-scale roughness amplitude (Brisset & Rémy 1996) and an improvement in the geometric boundary conditions (Bamber & Huybrechts 1996). In addition to these observations related to particular anomalies or rheological behaviour, the first large-scale topography derived from the 35-day repeat orbit allowed ice-flow modelling to be constrained and thus geophysical parameters to be estimated or fitted. With the help of such a topography, Budd & Warner (1996) compared the computed balance surface velocity and the observed deformation velocity in order to estimate rates of change of elevation. Rémy *et al.* (1996) estimated rheological values, and pointed out changes in flow regime due to ice temperature. Some physical processes can also be deduced from the topography. Rémy & Minster (1997) showed that the anomalies of the surface topography, due to the boundary flow conditions of glaciers, propagate from the coast up to the dome. This indicates the drainage pattern, upstream glacier positions or the flowline directions, and also the role of the outlet flow conditions of the whole ice sheet shape.

In April 1994, ERS-1 was moved to a geodetic 168-day repeat orbit of two shifted cycles in order to obtain a global mapping between 82°N and 82°S of the mean sea surface, until mid-March 1995. Previous altimetric measurements with such a high-density coverage (Geosat geodetic mission) had already been made, but were restricted to between 72°N and 72°S (Sandwell 1992). The first ERS high-resolution map of the mean sea surface that revealed the very fine structure of the marine geoid was produced by Cazenave *et al.* (1996). The spacing between satellite tracks of 8 km at the equator decreases to 1.5 km at 70°. Moreover, the raw altimeter data used for continental altimetric studies is given each 1/20 s, corresponding to a 350 m spacing along track. This very dense along- and across-track sampling allows us to recover the surface topography with a very high resolution. Comparisons of such a map with Landsat Thematic Mapper images around the ice stream of the Ross Ice Shelf have demonstrated the usefulness of the newly available fine-scale topographic data (Bamber & Bindschadler 1997).

The aim of this paper is to focus on the particular information contained in such a topography and to point out physical processes acting at the 10–20 km scale, which are not yet fully identified and understood.

2 DATA ANALYSIS

2.1 Data processing

We used the waveform altimeter product (WAP) delivered by the UK Processing and Archiving Facility (UK-PAF). The altimeter was in ice mode during the geodetic cycle. The ice-mode tracking is devoted to the tracking of steep topography, whilst ocean-mode tracking, having a bandwidth that is four times higher, is more accurate but is not able to follow the steep area of the ice sheet margins. Up to 30 million waveforms over Antarctica and 3 million over Greenland are available and were reprocessed. The small-scale topography signal causes a poor on-board tracking of the ground. This is corrected for by using the retracking algorithm developed in Féménias *et al.* (1993) and Legresy & Rémy (1997). Data editing and geophysical corrections are taken from Brisset & Rémy (1996). We used the Delft Institute precise orbit, and the altitude is given with respect to the WGS-84 ellipsoid.

2.2 Radial orbit error and crossover analysis

The crossover analysis and the height interpolation (next section) are taken from Cazenave *et al.* (1996), where these techniques are detailed. As the radial orbit error occurs at long wavelengths (Chelton & Schlax 1993), it is empirically modelled by adjusting simple functions such as polynomials or sinusoids along satellite profiles. It is then reduced by the procedure of crossover analysis. In contrast to the oceanic case, the temporal fluctuations of the ice sheet topography are negligible in comparison with the orbit error. However, snow surface characteristics exhibit variations due to changes in meteorological conditions, yielding artificial variations of a few tens of centimetres in height (Legresy & Rémy 1998), at a meteorological scale and a seasonal scale. Moreover, the orientation between antenna polarization and sastrugi direction partially affects the volume contribution of the altimetric return echo (Legresy & Rémy 1998). This effect contributes to the difference of height measurements between ascending and descending satellite ground tracks because of the difference in orientation between satellite ground tracks. This effect leads to a large stationary geographical signature, linked to the medium-scale topography orientation, and has an amplitude of 30 cm in areas of strong katabatic wind.

The crossover difference is minimized through a least-squares approach. In order to minimize the error due to the medium-scale orbit error, we process as long a track as possible (up to few thousand kilometres). The orbit error and the seasonal signal are then assumed to be well corrected, while the errors due to track orientation and the meteorological scale error are assumed to be minimized. Before adjustment, the rms crossover difference is 0.97 m over East Antarctica, 1.5 m over uneven West Antarctica and 0.75 m over the flat Ross and Ronne ice shelves. After adjustment, the rms crossovers are, respectively, 0.78 m, 1.3 m and 0.55 m. Therefore, the improvement is of the same order for the three regions (between 0.55 and 0.6 m), whilst the final error appears to be linked to the mean kilometre-scale roughness. Indeed, after retracking, the remaining white noise is mostly due to the complex convolution between volume echo and the kilometre-scale roughness that distorts the waveform shape (Wingham 1995; Legresy & Rémy 1997). Finally, we note that the rms after adjustment is not reduced by increasing the degree of freedom of the polynomial forms, indicating that the error associated with long-wavelength phenomena (mainly orbit) is well modelled.

2.3 Interpolation and slope error correction

The 30 million measurements over Antarctica and the 3 million over Greenland have been interpolated on a regular grid of $1/30^\circ \times 1/30^\circ$ mesh size, that is, around 3.5 km in latitude and from 1.3 to 0.6 km in longitude. This very high-resolution map is compatible with the along- and across-track sampling. We used commercial UNIRAS software for this purpose and selected a bilinear interpolation method. Data inside a circular area around a grid node were used for interpolation, and a search radius of 1/4° was considered.

At this point in the calculation, the slope-induced error can be corrected (Brenner *et al.* 1983). This error is due to the shift of the impact point in the upslope direction, and is the dominant error in altimeter heights of an ice sheet. This error is less than 0.5 m for regions where the slope is less than 0.05°, e.g. near domes or ice divides, but can reach a few metres elsewhere. This error depends on all surface derivatives. For each grid node, the slope and curvature are estimated by fitting a biquadratic form to the vicinity of the node and the correction is applied as explained in Rémy *et al.* (1989).

3 HIGH-RESOLUTION SURFACE TOPOGRAPHY: RESULTS AND DISCUSSION

3.1 General characteristics of ice sheet topography and surface slope

The high-resolution topographies of Antarctica and Greenland are shown Figs 1 and 2. Both maps unveil regular 10-km-scale roughness, but the Antarctic map also exhibits several impressive scars related to local flow anomalies. Most of them are located in Terre Adelie and Wilkes Land. On the close-up view (Fig. 3), one can identify lakes such as Vostok (105°E, 77°S) and Astrolabe (136°E, 69°S), inland slope breaks such as the Λ-shaped scar near (140°E, 75°S), 10-km-scale undulation networks that sometimes intermingle with each other (110°E, 73°S), and 60-km-scale undulations over the ice shelf (Fig. 4).

The surface slope (Figs 5 and 6) and its direction play a role in the estimation of the intensity and direction of the ice flow, and of the flow of katabatic winds. Same details, namely 10-km-scale undulations, lakes or scars, are also visible in these maps. At the large scale, the inland surface slope of Antarctica slowly increases from 0 to 3 m km^{-1}, before abruptly decreasing at a height of 2000 m. This slope break plays an important role in the ice dynamics and in the katabatic flow regime (Pettré *et al.* 1986).

The most striking feature is the irregular slope intensity at small scales, which raises the problem of the horizontal distance over which the slope parameter is to be averaged when applying the flow law. On a large scale, i.e. 20 times the ice thickness, shallow ice approximation to order 0 is valid (Morland 1984): the ice flow at any depth is directed along the steepest slope of the surface. The shear stress is dominant over other stresses and can be used for large-scale modelling. At a smaller scale, other stresses such as longitudinal stress can no longer be neglected. We will show that the small-scale behaviour of the surface slope then gives information on the physical characteristics that need to be taken into account.

The same is true of the katabatic flow: the effect of the undulations may be neglected only if the scale is smaller than 50 km (Kikuchi & Ageta 1989).

3.2 Ice shelves

Much of Antarctica is surrounded by large floating ice shelves. They are fed by ice flows from the grounded ice sheet and by snow accumulation, while ablation is principally due to iceberg calving and basal melting. The Ross Ice Shelf, shown in Fig. 4, is the largest shelf of Antarctica, with a surface of 525×10^3 km^2. The mean thickness varies from 1000 m where the ice starts to float (300 km south of the limit of the ERS data), to 250 m at the seaward margin. The ice velocity increases from a few hundred metres per year near the continent to 1000 m yr^{-1} near the edge (Rommelaere & MacAyeal 1997).

Some well-known topographic signatures of the glaciers already detected from AVHRR images (Casassa & Whillians 1994) and associated with their dynamics are also clearly visible. For instance, Byrd Glacier, which flows from East Antarctica into the Ross Ice Shelf near 80°S, 160°E, induces a positive anomaly up to 10 m high that is more than 200 km long. It is also true of the ice streams that drain out of the West Antarctica Ice Sheet, in particular ice streams D and E, which go north of Siple Dome (152°W, 81.5°S, the white area of the top left corner of Fig. 4). The positive topographic anomaly is strongly enhanced by the presence of the Roosevelt Ice island which breaks the flow. The whole ice shelf, like the whole ice sheet, is composed of adjacent and well-separated flowlines. These elongated topographic anomalies for the grounded ice sheet are due to outlet flow conditions that are transmitted from the coast up to the dome (Rémy & Minster 1997) and that are strongly persistent. On the other hand, in the ice shelf case these topographic anomalies arise from the difference in glacier velocity in the upstream direction, and their signatures are persistent only over a few hundred kilometres, that is, during around 1000 years.

The quasi-periodic variation of some of these topographic signature was pointed out by Bamber & Bindschadler (1997) on the western part of the shelf. They observed these quasi-periodic features in the flow direction and related this to regions of higher basal resistance. However, the topographic signature of the Nimrod Glacier (first glacier east of the Byrd glacier), coming from the south at longitude 165°E, also shows an unexpected periodic bumpy topography after its deflection to the right. At this location, the shelf is floating, so local variations of the friction cannot explain this. Moreover, one observes that the bumps have a 55 km even spacing and an oblique orientation of approximately 45° to the mean glacier direction, which corresponds to the well-known geological *en echelon* folds (see Sylvester 1988 for a review). These *en echelon* morphologies could be related to the faster flow coming from Beardmore and Lennox-King Glacier because its direction is in good agreement with left-lateral strike-slip and because bump morphologies are observed before the shear zone between the Nimrod and Byrd glaciers. The factors that control the style and development of these structures in simple shear have not been clearly defined. However, since the fold spacing, orientation, size and rate of growth depend on the cohesion of the ice, on the strain rate and on the degree of strike-slip convergence, their analysis may help to constrain the ice shelf rheology better.

3.3 Glacial lakes

Depending on ice thickness, geothermal flux and thermal dissipation, basal ice may reach the melting point in some places. If the basal bedrock slope is approximately 10 times that of the surface, then the pressure gradient is not sufficient to drive out the water. Such cases appear in Antarctica and were identified from radio echo sounding (Oswald & Robin 1973), for instance the Vostok Lake (see Figs 1 and 3 near 105°, from 76°S to 79°S), which has an impressive surface signature and whose true size was revealed by ERS altimetric observations (Ridley *et al.* 1993; Kapitsa *et al.* 1996). Sliding

Figure 1. High-resolution map of Antarctic Ice Sheet topography from the ERS1 geodetic mission. The grid size is 1/30°.

releases the basal shear stress producing a vanishing surface slope. However, one observes that the flat area is surrounded by two symmetrical dips. An enlargement of this area in the flow direction exhibits a trough between the lake and the upstream area and a symmetrical bump between the lake and the downstream area (Fig. 7). The trough was observed by Ridley *et al.* (1993) from the Fast Delivery data of an ERS track crossing this area, and compared to the flexure due to a

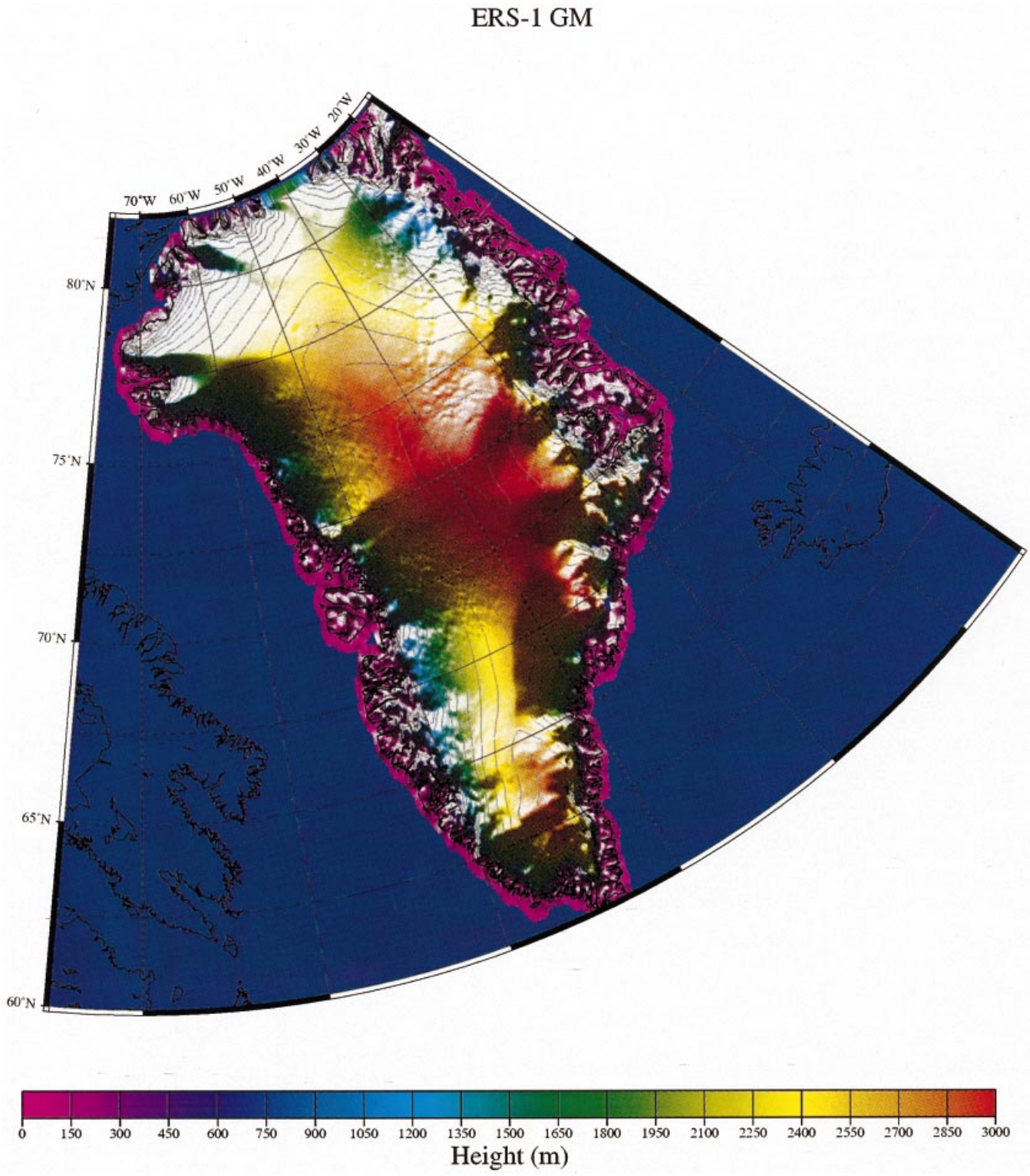

Figure 2. High-resolution map of Greenland Ice Sheet topography from the ERS1 geodetic mission. The grid size is 1/30°.

flow transition. Indeed such troughs are observed near ice stream grounding zones (Vaughan 1994) and are numerically generated when simulating an abrupt flow transition (Lestringant 1994). However, it is the first time that a transition between weak friction and strong friction (compression) and its inverse (extension) have been mapped so accurately. As the averaged upstream slope is of the same order of magnitude as the downstream slope, one can assume that the friction before and after the sliding area is of the same order, and thus that both opposite transitions lead to symmetrical topographic signatures. The whole transition takes place on a characteristic 20 km scale and yields a 6 m high anomaly (Fig. 7). The same analysis

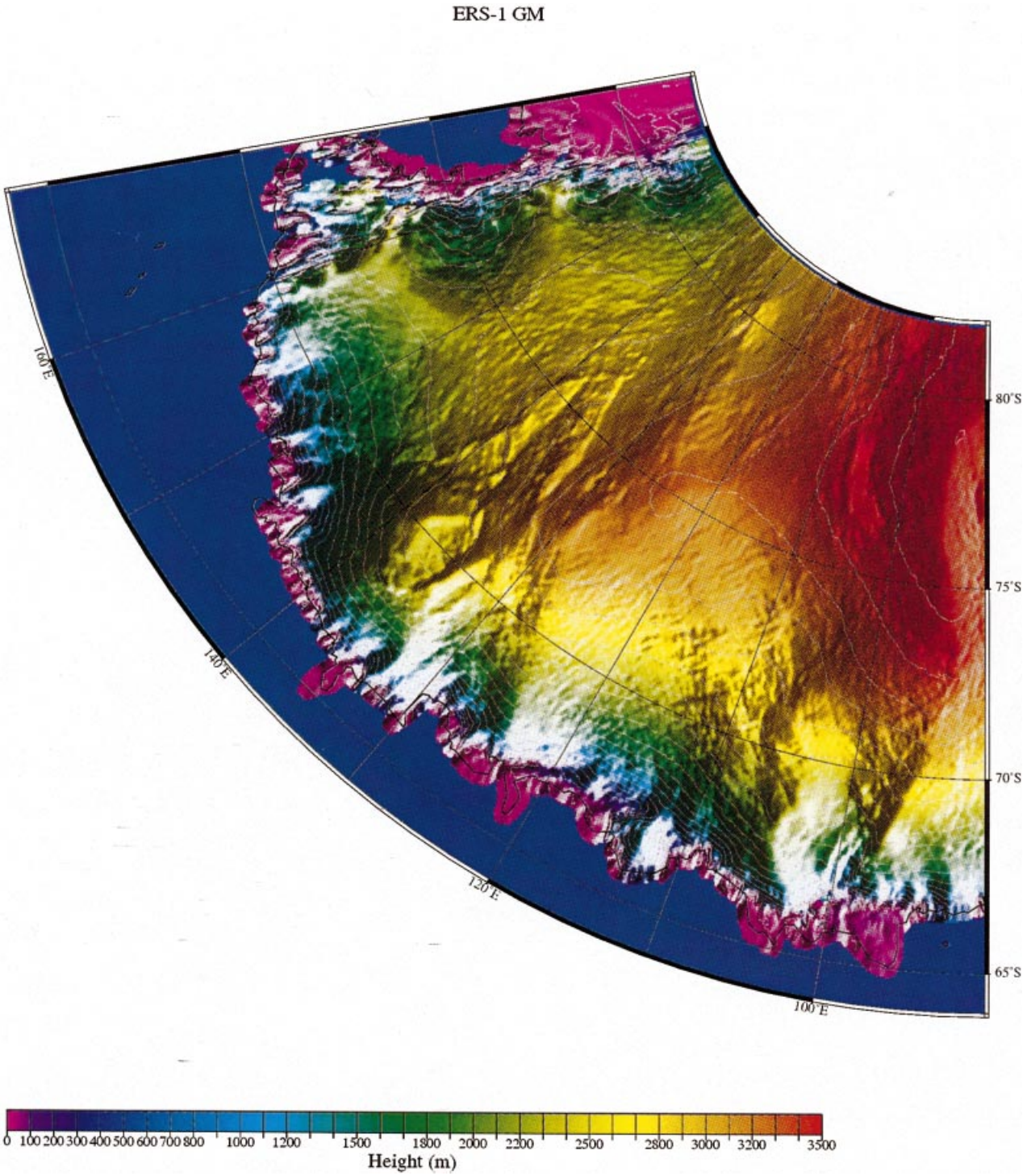

Figure 3. Close-up view of Terre Adélie and Wilkes Land. Several impressive scars related to local flow anomalies are visible, including 'lakes', a slope break and intersecting undulation networks.

was performed for the Astrolabe Lake (69°S, 136°E). This indicates a similar horizontal characteristic scale with a greater topography anomaly (12 m). This characteristic scale is actually much larger than that obtained by Shoemaker (1990) in his model of the transition zone. Also, his model only predicts a decrease of the surface topography.

However, Fig. 7 suggests that the transition between deformation and sliding occurs in two steps: a first step from km 5 to km 15 corresponding to a longitudinal extension, followed by a longitudinal compression from km 15 to km 25. Shoemaker (1990) only modelled the first transition part. A first-order analysis may explain the whole transition signature.

The steady-state equation, which can be applied at any scale, leads to

$$U\,dH + H\,dU = b\,dx\,, \tag{1}$$

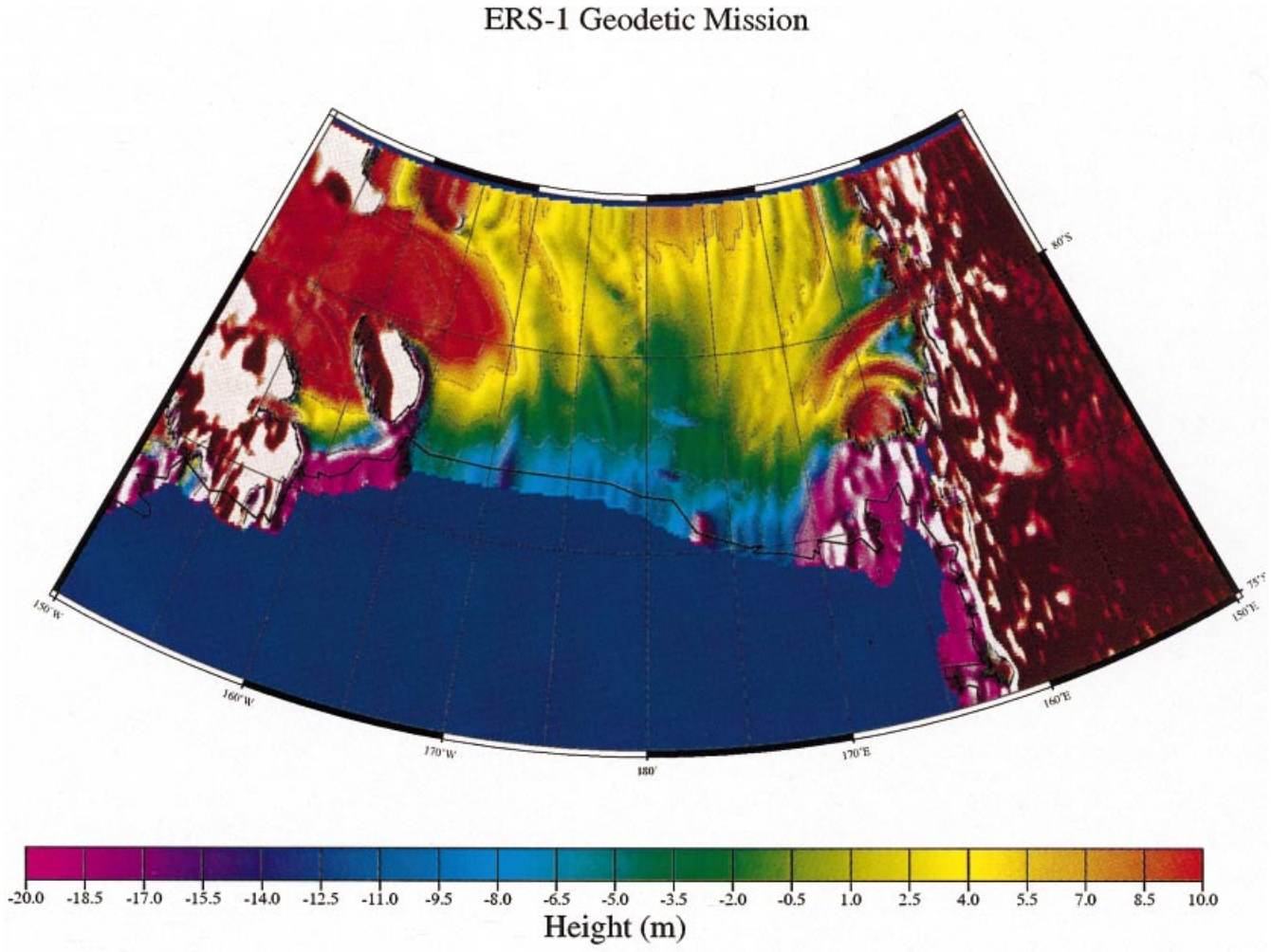

Figure 4. Close-up view of the Ross Ice Shelf. Note the impressive signature of glaciers draining West and East Antarctica, bumpy topography of one glacier coming from the south, and the negative topography anomaly in the middle of the shelf.

where U is the mean horizontal velocity, H is the ice thickness, b is the accumulation rate and x is the flow direction (with $U = 3$ m yr^{-1}, $H = 3800$ m and $b = 0.025$ g cm^{-2}, Kapitsa *et al.* 1996; Ritz 1989).

The derivative of the horizontal velocity with respect to x is given by the Glen law with $n = 3$:

$$dU/dx = A(\tau_{xz}^2 + \sigma_{xx}^2)\sigma_{xx}, \tag{2}$$

where τ_{xz} is the basal shear stress, σ_{xx} is the longitudinal stress and A is the flow law constant, 0.053 yr^{-1} bar^{-3}. Shoemaker (1990) assumed that the basal shear stress linearly decreased during the transition occurring at a length l_1, from τ_o to 0, and with the help of the mass equilibrium equation he derived the evolution of the longitudinal stress during the transition. Its mean horizontal value is given by

$$\sigma_{xx}(x) = \tau_o x/(4H)(2 - x/l_1) + \tau_o H/(12l_1). \tag{3}$$

At the end of the transition ice is floating over the lake. Indeed, we find σ_{xx} and then dU/dx are positive, corresponding to longitudinal extension. dU/dx deduced from eq. (2) allows the estimation of dH/dx using (1). If one assumes a transition length of 10 km, the corresponding height profile fits the data from km 5 to km 15 well. In this case, dU/dx is found to increase from 7.95×10^{-6} yr^{-1} [eq. (1) with $dH/dx = 1.5$ m km^{-1}] to 8.95×10^{-6} yr^{-1} at the end of the transition (eqs 2 and 3). However, the dU/dx value over the lake, where dH/dx is 0, must be 6.93×10^{-6} yr^{-1}. To reach the equilibrium, a second step is thus necessary, corresponding to a longitudinal compression.

The jump in ice thickness can be deduced from (1):

$$\Delta H = [b - H\Delta(dU/dx)]l_2/U; \tag{4}$$

due to the difference between the densities of ice and water, the corresponding height jump is given by (Kapitsa *et al.* 1996)

$$\Delta h = (1 - \rho_{ice}/\rho_{water})\Delta H. \tag{5}$$

If we assume that l_2 is around 10 km (Fig. 7) and $(1-\rho_{ice}/\rho_{water})$ is 0.1, then Δh is found to be 5.6 m. These values are in good agreement with observations. The scale at which longitudinal stress acts seems to be between 2 and 3 times the ice thickness, which is in good agreement with theory.

3.4 Surface undulations

The presence of undulations on the ice sheet surface has been attributed to the processes of the ice flow above irregular bedrock (Bourgoin 1956; Budd 1971). Robin (1967) explained surface slope fluctuations in terms of variations in the longitudinal stress that are produced by ice flow over the bedrock.

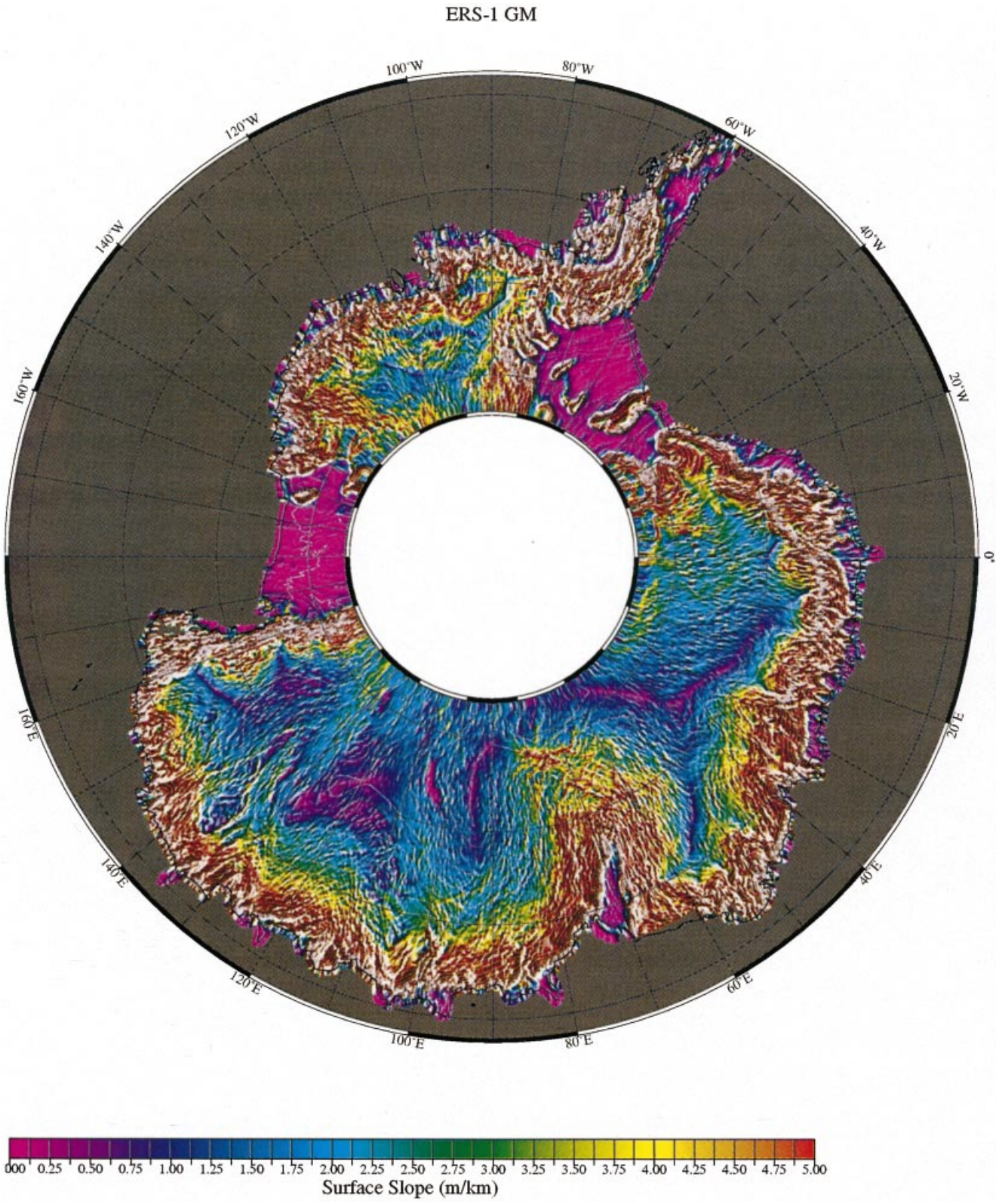

Figure 5. High-resolution map of the Antarctic Ice Sheet surface slope from the ERS1 geodetic mission. 'Lakes', domes and ice divides appear in mauve, whilst steep areas appear in red.

Budd (1970) defined a damping factor that describes the transfer of features in the basal topography to the ice surface and predicted a dominant response with wavelengths 3.3 times the ice thickness. On the other hand, Hutter *et al.* (1981) derived a filter function that defines the fraction of the bedrock amplitudes transmitted to the ice sheet surface as a function of wavelength and suggested an increasing surface response at longer wavelengths. A spectral analysis of the surface topography

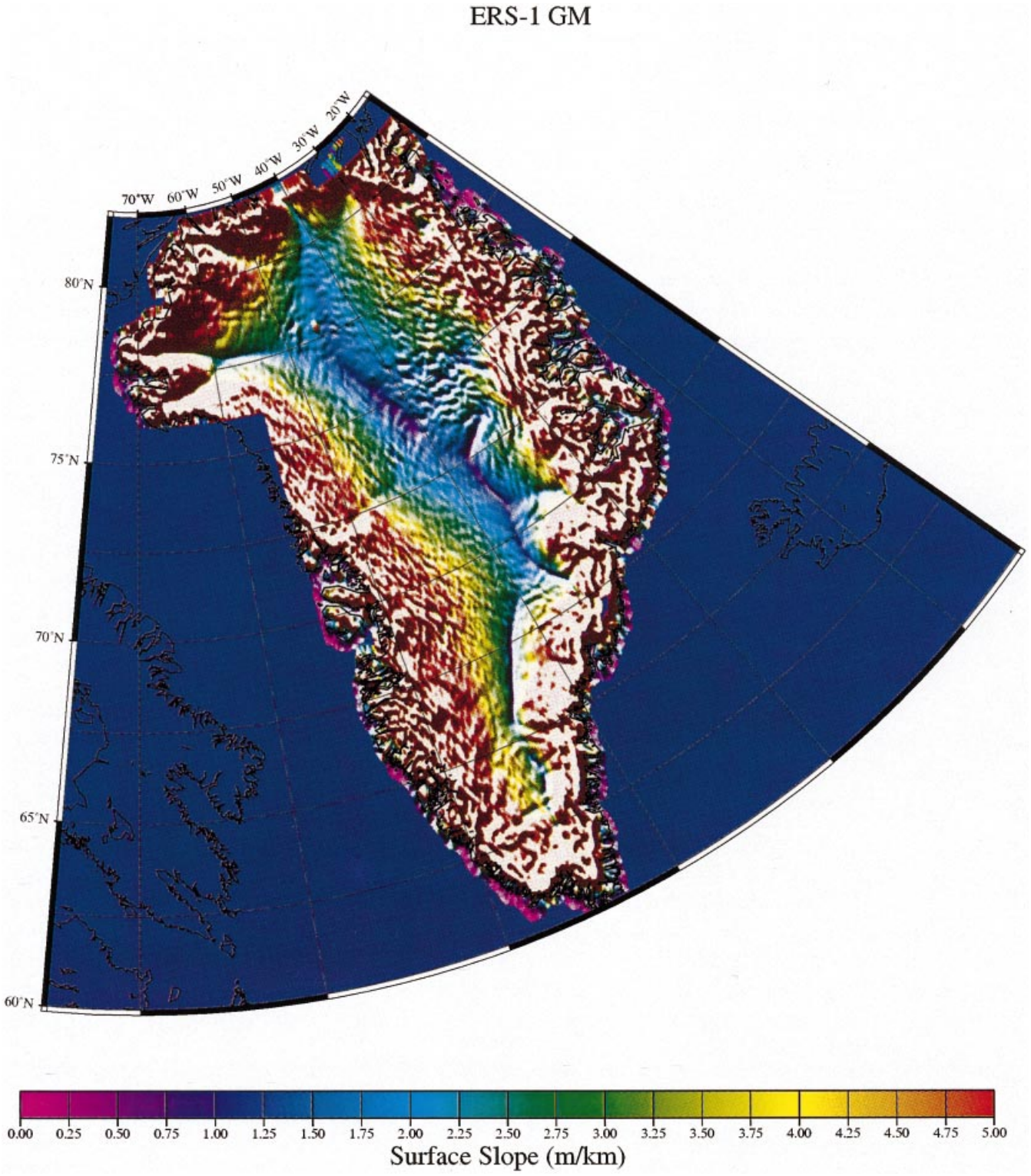

Figure 6. High-resolution map of the Greenland Ice Sheet surface slope from the ERS1 geodetic mission.

derived from airborne altimeters seems to confirm the greater response of the ice sheet to bedrock features with longer wavelengths (McIntyre 1986).

Undulating topography on the East Antarctic Ice Sheet is also clearly revealed by the NOAA Advanced Very High Resolution Radiometer (AVHRR). Using these data, Seko *et al.* (1993) showed that these features are associated with large variations of net accumulation rate. These authors attributed the surface undulations to snow redistribution by katabatic wind. However, a theoretical study of katabatic wind suggests that the wind is able to create a 40 km wavelength topography only after the slope break (Pettré *et al.* 1986).

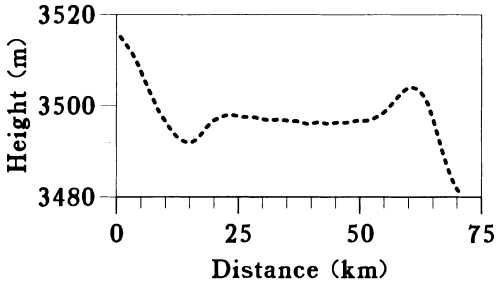

Figure 7. Cross-section of the Vostok Lake along latitude 78°. The basal lake corresponds to the flat area from km 10 to km 65. Note the transition between strong friction and weak friction, and vice versa.

McIntyre (1986) found that the distributions of small-scale surface gradients normal and parallel to flowlines are similar in form and magnitude, and modelled undulations such as symmetrical dome-shaped features. However, Figs 5 and 6 exhibit elongated undulations whose oblique orientation is frequently at 45° to the large-scale surface slope direction, assumed to be the flowline direction. In order to check that this orientation is not due to a data processing artefact, a 200 km × 400 km area is enlarged in Fig. 8 with closely spaced isocontour lines in order to show the undulations. The trailing edges of the altimetric waveforms for the ascending and descending passes are shown in Figs 8(a) and (b), respectively. The altimetric trailing edge is controlled at the large scale by the surface slope (Martin *et al.* 1983) and radar wave penetration within the snowpack (Ridley & Partington 1988) and by surface curvature at the radar footprint (i.e. 10 km) scale (Legresy & Rémy 1997). It thus provides an independent estimate of the surface curvature variations. The elongated features are also visible in this radar waveform parameter and confirm the main characteristics. These features are similar in ascending and descending pass data, demonstrating that this is not an artefact due to the difference between ascending and descending passes (Legresy & Rémy 1998).

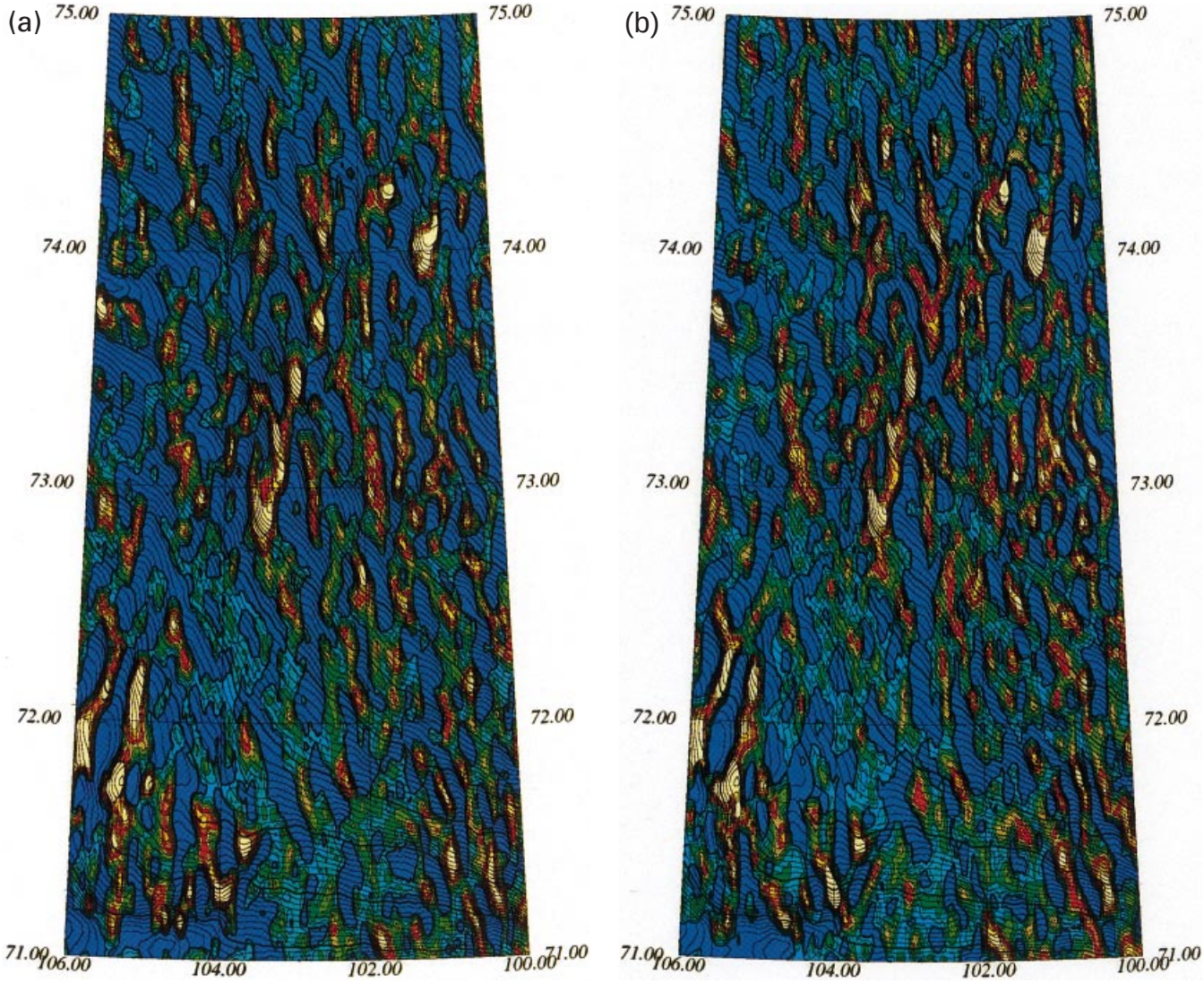

Figure 8. Enlargement of an undulating area. A radar waveform parameter affected by surface curvature is shown for (a) ascending and (b) descending passes. These undulations are thus neither an artefact from the topography construction or an artefact from the pass direction. The isolines of the superimposed topography are shown every 2 m. Note that the undulations are elongated and have an orientation of 45° with respect to the surface slope direction.

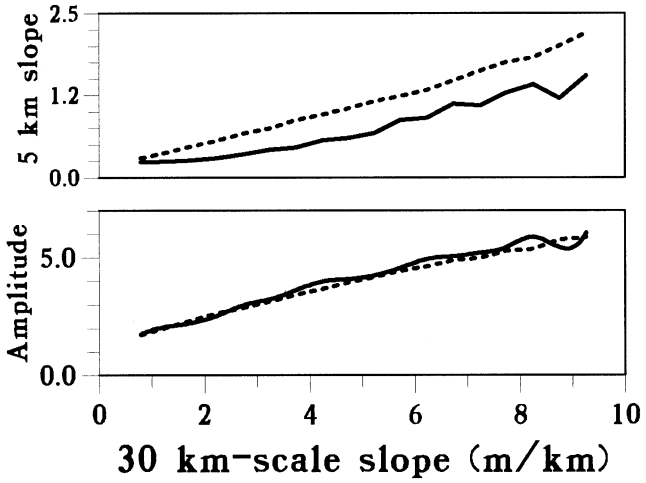

Figure 9. Main undulation characteristics of the Greenland Ice Sheet (solid lines) and the Antarctica Ice Sheet (in dashed lines). The amplitude (in m) and the 5-km-scale rms slope (m km^{-1}) are shown with respect to the large-scale surface slope.

The average characteristics of these undulations are displayed in Fig. 9, plotted as a function of the 30-km-scale surface slope (i.e. estimated at the 30 km scale), which increases regularly from the ice divide to the coast. The mean rms height is estimated by removing the 30-km-scale topography, while the mean 5-km-scale rms slope is estimated by removing the 30-km-scale slope. Both undulation amplitudes and the 5-km-scale slope increase linearly with the large-scale slope. The amplitude dependence on large-scale slope increases from 2 to 8 m, and is the same for both ice sheets; the 5-km-scale slope is slightly greater for Antarctica than for Greenland. If the shortest scale is modelled by a sinusoidal function $A \sin(2\pi/\lambda)$ of a given wavelength λ and amplitude A, then the wavelength can be given by the ratio between the rms height and the rms slope, multiplied by 2π. We found values of around 18 km for Antarctica and 20 km for Greenland.

No change in this behaviour is observed before and after the slope break (around 3.5 m km^{-1}). Features induced by katabatic winds are thus unlikely. Moreover, the similar behaviour of undulations in both ice sheets suggests that these undulations are related to ice flow rather than to katabatic winds. Finally, the wavelength is found to be quite constant, at around 18 km for the Antarctica Ice Sheet and 20 km for the Greenland Ice Sheet, in contradiction to the theory of Budd (1970). This theory predicts a dominant response with wavelengths 3.3 times the ice thickness.

4 CONCLUSIONS

In this paper we have presented new high-resolution ice sheet topography maps derived from altimeter data from the ERS-1 altimeter geodetic mission. The waveform altimeter products were reprocessed with a dedicated algorithm, the radial orbit error was reduced by using a crossover analysis, and the slope error was corrected, taking into account surface slope and curvature. The maps were generated with a high resolution of 1/30°. They provide a detailed topography description from which processes that act on ice flow may be inferred and may help in their understanding and modelling. Many scars related to ice flow are exhibited: lakes, inland slope breaks, glacier flowlines, *en echelon* structures and undulations. Some details of these topographic signatures were noted for the first time, for instance the presence of the *en echelon* structure of the ice shelf or the characteristic orientation of the undulations.

Topographic signatures of the flat ice shelf allowed the distinction of adjacent glaciers and allowed us to see lateral stress effects. *En echelon* structures with an oblique orientation at 45° with respect to the flow direction were found.

Local sliding areas such as 'lakes' seem to be surrounded by two symmetrical topographic anomalies. Bumps and troughs on the topography are associated with abrupt transition from weak to strong friction and from strong to weak friction, respectively. We quantitatively showed that these transitions occur in two steps, longitudinal extension followed by longitudinal compression for a transition between deformation and sliding, and vice versa. All characteristic scales of the longitudinal variations are around 10 km. This scale corresponds to the scale at which longitudinal stress acts.

In the same way, the 10-km-scale undulations seem to be the main ice sheet surface features. Up to now, they have been modelled as symmetrical dome-shaped features. Their spatial characteristics pointed out in this paper will allow a better understanding and modelling of these networks. They are found to be elongated, frequently oriented at 45° to the flowline directions. Their amplitude and 5-km-scale slope in the shortest direction increase linearly with surface slope. Finally, the 10 km scale seems to be a characteristic scale of ice flow processes. The similarity between the scale of the transition zone and that of the undulations, and the similarity between the orientation of the *en echelon* structures and that of the undulation networks may prove useful in investigating these features more closely.

Several other glaciological investigations may be conducted using this data set. No other geodetic mission is planned in the near future, and such topographies will remain of importance for a long time. In particular, they will represent a basis for any long-term survey of the ice sheet volume.

REFERENCES

Bamber, J.L. & Bindschadler, R.A., 1997. An improved elevation dataset for climate and ice-sheet modelling: validation with satellite imagery, *Ann. Glaciol.,* **25,** 439–444.

Bamber, J.L. & Huybrechts, P., 1996. Geometric boundary conditions for modelling the velocity field of the Antarctic ice sheet, *Ann. Glaciol.,* **23,** 364–373.

Bourgoin, J.P., 1956. Quelques caractères analytiques de la surface et du socle de l'Inlandsis groenlandais, *Ann. Géophys.,* **12,** 75–83.

Brenner, A.C., Bindschadler, R.A., Thomas, R.H. & Zwally, H.J., 1983. Slope induced errors in radar altimetry over continental ice sheets, *J. geophys. Res.,* **88,** 1617–1623.

Brisset, L. & Rémy, F., 1996. Antarctica surface topography and kilometric scale features derived from ERS-1 satellite altimeter, *Ann. Glaciol.,* **23,** 374–381.

Brooks, R.L. & Norcross, G.A., 1982. *East Antarctica Ice Sheet Surface Contours from Satellite Radar Altimetry,* Geoscience Research Corporation, Salisbury, MD.

Budd, W.F., 1970. Ice flow over bedrock perturbations, *J. Glaciol.,* **10,** 177–195.

Budd, W.F., 1971. Stress variations with ice flow over undulations, *J. Glaciol.,* **9,** 29–48.

Budd, W.F. & Warner, R.C., 1996. A computer scheme for rapid calculations of balance-flux distributions, *Ann. Glaciol.,* **23,** 21–27.

Casassa, G. & Whillians, I., 1994. Decay of surface topography on the Ross Ice Shelf, Antarctica, *Ann. Glaciol.,* **20,** 249–253.

Cazenave, A., Schaeffer, P., Berge, M., Brossier, C., Dominh, K. & Gennero, M.C., 1996. High-resolution mean sea surface computed with altimeter data of ERS-1 (geodetic mission) and Topex-Poseïdon, *Geophys. J. Int.,* **125,** 696–704.

Chelton, D.B. & Schlax, M.G., 1993. Spectral characteristics of time-dependent orbit errors in altimeter height measurements, *J. geophys. Res.,* **98,** 12 579–12 600.

Cudlip, W. & McIntyre, N., 1986. Seasat altimeter observations of an Antarctica lake, *Ann. Glaciol.,* **9,** 55–59.

Féménias, P., Rémy, F., Raizonville, P. & Minster, J.-F., 1993. Analysis of satellite altimeter height measurements above an ice sheet, *J. Glaciol.,* **133,** 591–600.

Glen, J.W., 1955. The creep of polycrystalline ice, *Proc. R. Soc. London,* A **228,** 519–538.

Hutter, K., Legerer, F. & Spring, U., 1981. First order stresses and deformations in glaciers and ice sheets, *J. Glaciol.,* **27,** 227–270.

Kapitsa, A.P., de Ridley, J.K.Q., Robin, G., Siegert, M.J. & Zotikov, I.A., 1996. A large deep freshwater lake beneath the ice of central Antarctica, *Nature,* **381,** 684–686.

Kikuchi, T. & Ageta, Y., 1989. A preliminary estimate of inertia effects in a bulk model of katabatic wind, *Proc. NIPR Symp. Polar Meteorol. Glaciol.,* **2,** 61–69.

Legresy, B. & Rémy, F., 1997. Surface characteristics of the Antarctic ice sheet and altimetric observations, *J. Glaciol.,* **43,** 265–275.

Legresy, B. & Rémy, F., 1998. Using the temporal variability of the radar altimetric signal to map surface characteristics of the Antarctic ice sheet, *J. Glaciol.,* **44,** 197–206.

Lestringant, R., 1994. A two-dimensional finite-element study of flow in the transition zone between an ice sheet and an ice shelf, *Ann. Glaciol.,* **20,** 67–73.

Martin, T.V., Zwally, H.J., Brenner, A.C. & Bindschadler, R.A., 1983. Analysis and retracking of continental ice sheet radar altimeter waveforms, *J. geophys. Res.,* **88,** 1608–1616.

McIntyre, N.F., 1986. The Antarctic ice sheet topography and surface bedrock relationship, *Ann. Glaciol.,* **8,** 124–128.

Morland, L.W., 1984. Thermo-mechanical balance of ice sheets flows, *J. Geophys. Astrophys. Fluid Dyn.,* **29,** 237–266.

Orovan, E., 1949. Remarks at joint meeting of the British Glaciological Society, the British Rheologists Club and the Institute of Metals, *J. Glaciol.,* **1,** 231–236.

Oswald, G.K.A. & Robin, Q. de G., 1973. Lakes beneath the Antarctic ice sheet, *Nature,* **245,** 251–254.

Pettré, P., Pinglot, J.F., Pourchet, M. & Reynaud, L., 1986. Accumulation distribution in Terre Adelie, Antarctica: effect of meteorological parameters, *J. Glaciol.,* **32,** 486–500.

Rémy, F. & Minster, J.-F., 1997. Antarctica ice sheet curvature and its relation with ice flow and boundary conditions, *Geophys. Res. Lett.,* **24,** 1039–1042.

Rémy, F., Mazzega, P., Houry, S., Brossier, C. & Minster, J.-F., 1989. Mapping of the topography of continental ice by inversion of satellite altimeter-data, *J. Glaciol.,* **35,** 98–107.

Rémy, F., Ritz, C. & Brisset, L., 1996. Ice sheet flow features and rheological parameters derived from precise altimetric topography, *Ann. Glaciol.,* **23,** 277–283.

Ridley, J.K. & Partington, K.C., 1988. A model of satellite radar altimeter return from ice sheets, *Int. J. Rem. Sens.,* **9,** 601–624.

Ridley, J.K., Cudlip, W. & Laxon, S., 1993. Identification of sub-glacial lakes using ERS-1 radar altimeter, *J. Glaciol.,* **39,** 625–634.

Ritz, C., 1989. Interpretation of the temperature profile measured at Vostok, East Antarctica, *Ann. Glaciol.,* **12,** 138–144.

Robin, G. de Q., 1967. Surface topography of ice sheets, *Nature,* **215,** 1029–1932.

Rommelaere, V. & MacAyeal, D.R., 1997. Large-scale rheology of the Ross Ice shelf, Antarctica, computed by a control method, *Ann. Glaciol.,* **24,** 43–48.

Sandwell, D.T., 1992. Antarctic marine gravity field from high density satellite altimetry, *Geophys. J. Int.,* **109,** 437–448.

Seko, K., Furukawa, T., Nishio, F. & Watanabe, O., 1993. Undulating topography on the Antarctic ice sheet revealed by NOAA AVHRR images, *Ann. Glaciol.,* **17,** 55–62.

Shoemaker, E.M., 1990. The ice topography over subglacial lakes, *Cold Regions Sci. Technol.,* **18,** 323–329.

Sylvester, A.G., 1988. Strike-slip faults, *Geophys. Soc. Am. Bull.,* **100,** 1666–1703.

Vaughan, D.G., 1994. Investigating tidal flexure on an ice shelf using kinematic GPS, *Ann. Glaciol.,* **20,** 372–376.

Wingham, D.J., 1995. A method for determining the average height of a large topographic ice sheet from observations of the echo received by a satellite altimeter, *J. Glaciol.,* **41,** 125–141.

Zwally, H.J., Bindschadler, R.A., Brenner, A.C., Martin, T.V. & Thomas, R.H., 1983. Surface elevation contours of Greenland and Antarctic ice sheets, *J. geophys. Res.,* **88,** 1589–1596.